Soft Electronic Materials MRes

Module 2

Section: Halide Perovskites

Julie Euvrard

Imperial College London

Autumn Term 2024

Lecture 1: Halide Perovskites - The basics	18/11/24
Lecture 2: Halide perovskite thin film growth	18/11/24
Lecture 3: Halide perovskite thin film characterisation	29/11/24
Lecture 4: Mastering defects in halide perovskites	29/11/24

IMPERIAL

Lecture 1: Halide Perovskites - The basics

Introduction

In this series of four lectures, we will take a closer look at halide perovskites. The goal is to lay the foundations of this class of materials, and understand how it relates to classical inorganic semiconductors (such as silicon) and organic semiconductors. Lecture 1 is an introduction to the topic of halide perovskites.

Contents

Why do we care?

In the quest for cheaper optoelectronic devices, including solar cells, soft electronic materials have gained tremendous traction. Halide perovskites score high in this category, especially for solar energy applications. Yet, work remains to be done before perovskite-based devices can be commercialised. Knowledge is the first step towards this development.

1 What crystals are halide perovskites?

The word **'perovskite'** designates a specific crystal structure adopted by the mineral $CaTiO_3$ and displayed in Fig. 1.1 where A=Ca, B=Ti and X=O. This crystal arrangement exhibits **corner-sharing** TiO_6 octahedra in three dimensions (3D), with Ca occupying the centre of each unit cell. Any crystal adopting this arrangement with chemical formula ABX_3 is called perovskite. We will see later that the term perovskite can be used more widely for crystals with corner-sharing arrangements in 2D and 1D.

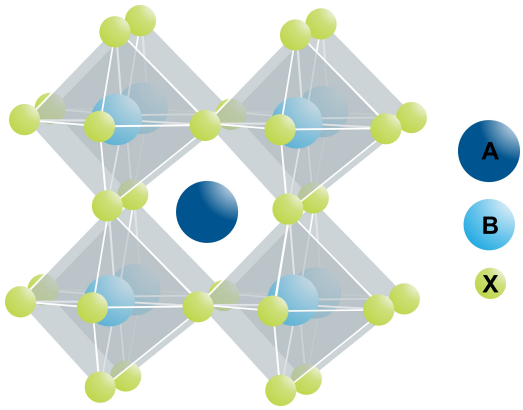

Figure 1.1: Schematic of the perovskite crystal structure with chemical formula ABX_3.

The perovskite structure can take different **crystal phases** depending on the relative position of the BX_6 polyhedra: cubic, tetragonal, orthorhombic, trigonal and monoclinic Bravais lattices. Phase changes can be induced by varying temperature or pressure. X-ray diffraction (XRD) is commonly used to determine the crystal phase of the perovskite (see Lecture 3).

1.1 Charge neutrality

As with any solid, **charge neutrality** must be ensured. Let's call q_A, q_B and q_X the charge of each atomic component. A stoichiometry of ABX_3 implies:

$$q_A + q_B + 3q_X = 0. \tag{1.1}$$

In the case of $CaTiO_3$, the **oxidation state** of each element is $q_{Ca} = 2+$, $q_{Ti} = 4+$ and $q_O = 2-$. Variations in the oxidation states between the A,B, and X components can be considered, as long as charge neutrality is conserved.

In the case of halide perovskites, generally opposed to perovskite oxides, X is occupied by an halogen (hence the term halide) such as iodine (I) or bromine (Br) with oxidation state $q_I = q_{Br} = 1-$. From equation 1.1 we deduce $q_A + q_B = -3q_X = 3+$. The only possible ternary combination in 3D halide perovskites is I-II-X_3 where $q_A = 1+$, $q_B = 2+$, and $q_X = 1-$ (e.g., $CsSnI_3$). Interestingly, the cation site A may be occupied by an organic molecule such as methylammonium CH_3NH_3, also written 'MA', forming **hybrid organic-inorganic perovskites 'HOIP'** (e.g., $MAPbI_3$). The B site is traditionally occupied by divalent metal cations such as lead (Pb) and tin (Sn).

By now you should realise a first interesting aspect of perovskite materials: they are very *versatile*. Given the large degree of freedom in composition, one may tune physical properties and search for the ideal semiconductor. Of course, there must be some constraints in the perovskite composition to ensure its characteristic crystal structure. You can for example imagine that a cation too large to fit within the cavity would disrupt the octahedra framework. An A cation too small would lead to a collapse of the inorganic framework.

1.2 Tolerance factor

Ionic size constraints determine the existence of a perovskite framework for a given set 'A-B-X'. The **Goldschmidt's Tolerance Factor** t is defined considering all ions as rigid spheres with radius R_A, R_B and R_X:

$$(R_A + R_X) = t\sqrt{2}(R_B + R_X) \tag{1.2}$$

with $t \sim 1$. It has been empirically demonstrated that a tolerance factor within the range $0.8 \leq t \leq 1$ allows the formation of the perovskite structure, and its specific value may inform on the most likely crystal phase. While $t = 1$ would guarantee a perfect fit of the cation 'A' between the BX_6 octahedra, and therefore a cubic structure, a lower value of t implies crystal lattice distortion. On the contrary, $t > 1$ corresponds to a cation 'A' to large to fit in the cavities usually preventing the formation of '3D' perovskites (see next section).

In addition, the **octahedral factor** μ assesses whether the 'B' atom will favour an octahedral coordination of 'X' atoms, and is defined by:

$$\mu = \frac{R_B}{R_X}. \tag{1.3}$$

The octahedral condition is satisfied for values of μ ranging from 0.4 to 0.8.

This versatility in composition offers the opportunity to finely tune the optical properties of the targeted semiconductor. For example, the bandgap of $MAPb(Br_xI_{1-x})_3$ can be tuned between 1.53 eV and 2.24 eV by mixing two halides, iodine and bromine, with various ratios x (Fig. 1.2).

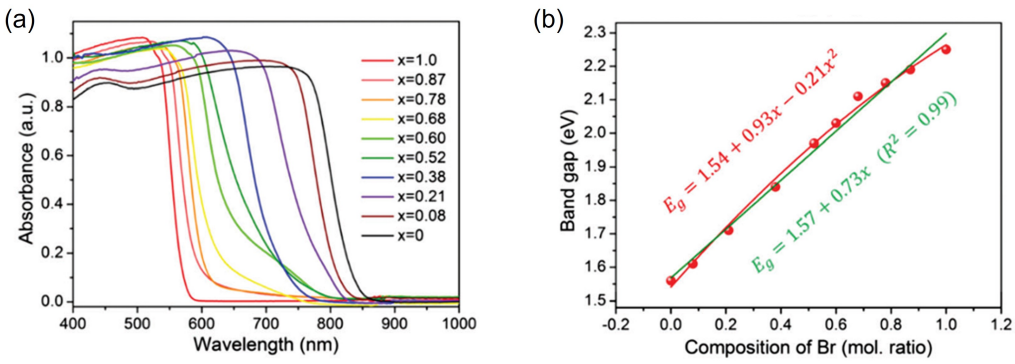

Figure 1.2: Absorption spectra (a) and extracted bandgaps (b) of $MAPb(Br_xI_{1-x})_3$ (x=0-1).[1]

[1] Zhang, Y., *et al.* (2016). *Journal of Materials Chemistry C*, 4(39), 9172-9178.

1.3 Beyond 3D perovskites

In practice, a perovskite structure can be maintained for $t > 1$, i.e., with a cation A too big to fit between the octahedra. In this situation, the 3D framework is disrupted to accommodate the larger cation (Fig. 1.3). This disruption leads to the formation of inorganic sheets with BX_6 octahedra separated by large organic cations. Since corner sharing of the octahedra only takes place in plane, this family of materials is known as **2D perovskites** or **layered perovskites**. Note, however, that layered perovskites are not 2D in the classical sense as used with graphene, but remain a bulk material. Between the two extreme cases of '3D' and '2D' perovskites lie **quasi-2D perovskites** (Fig. 1.3c), where multiple layers (n) of octahedra with small cations are separated by sheets of larger organic cations.

2D and quasi-2D perovskites are divided in two categories: **Ruddlesden-Popper (RP)** and **Dion-Jacobson (DJ)**. In RP perovskites, inorganic sheets are linked by two layers of organic cations separated by a van der Waals gap. In DJ perovskites, only one layer of organic cation links the two sheets of octahedra. The general chemical formula of RP and DJ perovskites are $A'_2A_{n-1}B_nX_{3n+1}$ and $A'A_{n-1}B_nX_{3n+1}$, respectively, where A' is the large organic cation.

We will not enter in the details of layered perovskites in this short set of lectures, but may refer to them in specific parts.

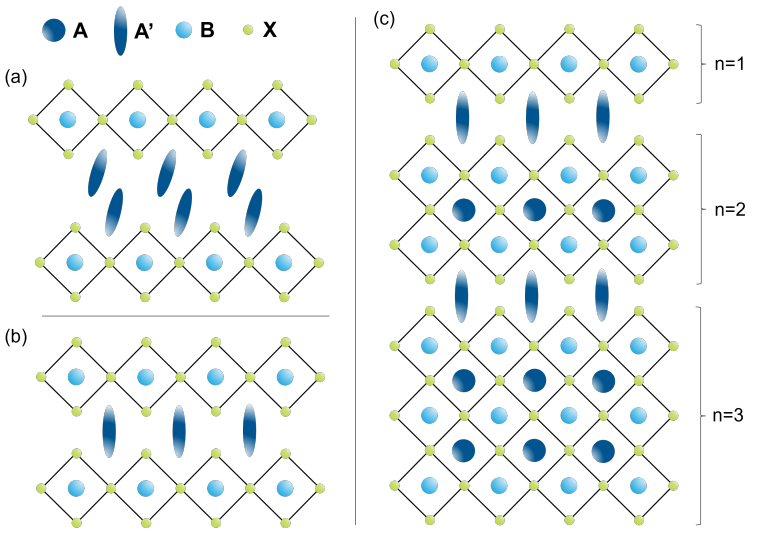

Figure 1.3: Schematic of (a) 2D Ruddlesden-Popper perovskite, and (b) 2D Dion-Jacobson perovskite. Schematic view of quasi-2D perovskite structure with n=1, 2, and 3.

2 Why are halide perovskites interesting?

Pb-based 3D halide perovskites (e.g., $MAPbI_3$) combine several key factors allowing their use as efficient solar absorbers:

- *High optical absorption*: A thickness of a few 100s of nm is sufficient to absorb most of the visible light, allowing for flexible applications.
- *Small effective masses for electrons and holes*: Charge carrier mobilities are reasonably high for solar cell applications.
- *High formation energy for deep defects*: The concentration of deep trap states is low, therefore limiting charge carrier recombination.

2.1 Electronic structure

What makes Pb-based halide perovskites so special is their electronic structure. As you may know from solid state or semiconductor physics, semiconductors and insulators differ from metals by the existence of an energy gap, **bandgap**, between a filled energy band, the **valence band**, and an empty energy band, the **conduction band**. The difference between semiconductors and insulators arises from the magnitude of the bandgap. A semiconductor's bandgap typically lies below 3 eV, providing them with higher conductivities ($10^{-9}\ S.cm^{-1} < \sigma_{SC} < 10^{2}\ S.cm^{-1}$) than insulators ($\sigma_{ins} < 10^{-9}\ S.cm^{-1}$) through thermal activation of carriers from the valence band to the conduction band.

A key parameter in the properties of semiconductors is the shape of the bottom of the conduction band and top of the valence band, which directly determines the **effective mass** m^* of the electrons and holes (m_e^* and m_h^*), and therefore their **mobility** (Fig. 1.4). The magnitude of the effective mass results from the interaction of electrons/holes with the periodic lattice and is related to the **electronic dispersion relation** $E(k)$ for parabolic bands according to:

$$m^* = \hbar^2 \left(\frac{d^2E}{dk^2} \right)^{-1}. \tag{1.4}$$

As a quick reminder, electronic dispersion relations relates the electron energy E with its momentum $p = \hbar k$ in a crystalline solid. A strong curvature in the $E(k)$ dispersion, called **'dispersive band'**, would indicate a small effective mass, and therefore an efficient transport with the mobility μ given by:

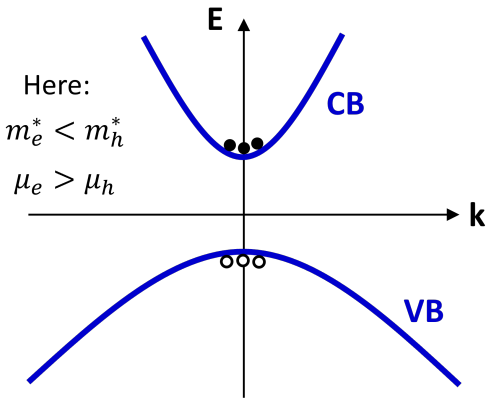

Figure 1.4: Energy dispersion diagram for a given semiconductor with a conduction band more dispersive than its valence band. This scenario would result in a lower electron effective mass and a larger electron mobility compared to holes.

$$\mu = \frac{q\tau_s}{m^*}, \tag{1.5}$$

where q is the elementary charge and τ_s the mean free time or average scattering time. On the contrary, a **'flat band'** near the band edge would result in heavier effective masses and inefficient charge transport with lower mobilities.

To predict charge transport in halide perovskites, we need to know which atomic orbitals are responsible for the valence band maximum (VBM) and conduction band minimum (CBM). In Pb-based halide perovskites, the VBM is determined by the Pb s and I p orbitals, while the Pb p orbital contribute to the CBM (Fig. 1.5). This contrasts from traditional semiconductors such as GaAs and CdTe which exhibit an opposite band structure where the CBM has strong s orbital character and the VBM a strong p orbital character. High energy s-orbitals are more delocalised than low energy p orbitals, implying that a smaller effective mass for electrons compared to holes in traditional semiconductors. In Pb-based halide perovskites, the lone pair Pb s electrons forms strong antibonding coupling with I p, making the upper valence band of $MAPbI_3$ dispersive and leading to a small hole effective mass. Therefore, the electron and hole effective masses are balanced ($m_e^* \sim m_h^* \sim 0.2 - 0.3 m_0$ for $MAPbI_3$, with m_0 the free electron mass) leading to **ambipolar conductivity**, which is favourable for pin-solar cell structures to enable efficient extraction of both types of charge carriers. You will note that the organic cation does not contribute to the states near the band edge, and therefore does not directly influence the transport and optoelectronic properties of the semiconductor.

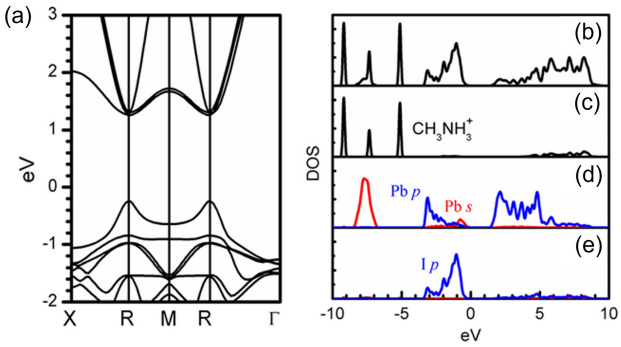

Figure 1.5: (a) Band structure of $MAPbI_3$. Total (b) and partial density of states (DOS) of MA (c), Pb (d), and I (e).[2]

In addition to charge transport, the optical absorption of a material is also closely related to its electronic structure. The **direct bandgap** of Pb-based halide perovskites is a key advantage over silicon and its indirect bandgap. Moreover, the **density of states** (DOS) near the CBM of halide perovskites is significantly higher than for GaAs (Fig. 1.6a), leading to a larger **joint density of states** (JDOS). Finally, the intra-atomic transition Pb s (VBM) to Pb p (CBM) benefits from a high probability. Therefore, combined contribution of high JDOS and probability of transitions ensures strong optical absorption (Fig. 1.6b). As a consequence, thin films of $MAPbI_3$ with a thickness no larger than ~300 nm are necessary to absorb most of the visible light, compared to thicknesses of ~2 µm required for most common thin film solar cell technologies (GaAs, CdTe, CIGS...).

[2]Yin, W. J., *et al.* (2014). *Applied Physics Letters*, 104(6).
[2]Yin, W. J., *et al.* (2014). *Advanced materials*, 26(27), 4653-4658..

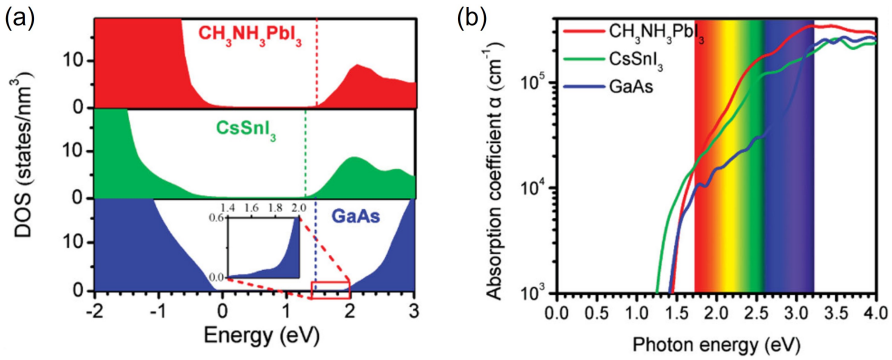

Figure 1.6: DOS (a) and optical absorption coefficient (b) of $MAPbI_3$, $CsSnI_3$, and GaAs. In the DOS, the zero energy corresponds to the VBM and CBMs are marked by dashed lines.[3]

2.2 Favourable defect chemistry

The existence and density of a given type of defects depends on its **formation energy** (concept explained in Lecture 4) which is determined by environmental factors such as precursor composition, partial pressure, and temperature during crystal growth. We will see more about the physics of perovskites defects in Lecture 4, and how its mastering can lead to electronic control. We will however note now the following peculiarities about defect chemistry in Pb-based halide perovskites:

- Deep defects have high formation energies.
- Dominant defects with low formation energies are shallow defects.
- Grain boundaries in polycrystalline films do not generally lead to the formation of deep defects.

These properties make Pb-based perovskites particularly robust for optoelectronic applications despite the low-temperature solution-based processes used, and explain why the field of perovskite solar cells has been so fruitful over the last decade.

3 What are the major challenges?

Despite the remarkable optoelectronic properties of Pb halide perovskites, some major challenges remain. Here we list a few of these challenges/issues:

- **Instability:** The ability of a material to persist in the desired phase under ambient condition is called **structural stability**. As a low formation energy is required to form a perovskite phase, allowing for low temperature processing, a low energy can also disrupt or dismentle the perovskite structure. The phase targeted and reached during film processing and crystal growth may be different from the thermodynamically most stable phase when exposed to various **stressors** such as temperature, light (especially UV), voltage bias, humidity, oxygen, and mechanical (strain). While a complete overview of the topic would require a set of several lectures, note that hybrid organic-inorganic perovskites such as $MAPbI_3$ are particularly unstable under thermal stress and decompose above temperatures of 80-100 °C. In addition to heat, halide perovskites are strongly impacted by humidity which leads to decomposition. Electrical stress can also be an important issue in perovskite devices, sometimes triggering redox reactions at interfaces. Our ability to stabilise the halide perovskite phase and increase its robustness to stressors will be key to the development of perovskite-based technologies.
- **Ionic motion:** Chemical bonding in halide perovskites is primarily ionic and is at the origin of the softness of the lattice. **Charged ionic defects** can become mobile through a vacancy-mediated transport process. High ionic conductivity results in current-voltage (I-V) measurements exhibiting a hysteresis as the device retains some memory of the previous biasing conditions. One major impact of ionic motion is the screening of the internal electric field which impedes efficient charge carriers

extraction.

- **Lead toxicity:** Current high efficiency perovskite solar cells are based on lead (Pb) as metal cation. To replace Pb, **homovalent** (e.g., Sn and Ge) and **heterovalent** (e.g., Bi and Sb) elements are considered. With the use of heterovalent atoms, charge neutrality is ensured with mixed cations to form $A_2B(I)B(III)X_6$, or the use of vacancies (symbol: □) leading to $A_3\square B(III)_2X_9$ and $A_2\square B(IV)X_6$. While the homovalent replacement leads to instability issues (oxidation), heterovalent replacement results in inferior optoelectronic properties. Therefore, achieving high solar cell efficiencies with Pb-free perovskites remains a challenge.
- **Electronic tunability:** As we will see in Lecture 4, halide perovskites are particularly challenging to dope both p- and n-type. One of the underlying reasons is associated with the softness of the lattice and the ability to compensate defects. Hence, what makes these materials resistant to defects, also makes them difficult to dope.

Timeline - Towards record solar cell efficiencies (non-examinable)

- **1839**: $CaTiO_3$ discovered by the Prussian mineralogist Gustav Rose in the Ural Mountains and named in honour of the Russian mineralogist Lev A. Perovskiy.
- **1893**: First synthesis of all inorganic halide perovskites.
- **1941**: Discovery of $BaTiO_3$. This perovskite oxide is the first ferroelectric ceramics and marks the beginning of perovskite research for electronic applications.
- **1978**: Dieter Weber (University of Stuttgart, Germany) synthesized the first hybrid organic-inorganic perovskite (HOIP).
- **1994-1999**: Exploration of the semiconducting properties of HOIP and discovery of electricity-to-light conversion ability by David Mitzi *et al.* (IBM, USA).[a][b]
- **2009**: First peer-review article reporting the use of halide perovskite in a dye-sensitized solar cell (DSSC) by Miyasaka *et al.*,[c] reaching a power conversion efficiency (PCE) of 3.8%.
- **2012**: Development of solid-state perovskite DSSC with a PCE of 9.7% by Park and Grätzel *et al.*,[d] and 7.6% by Snaith *et al.*[e]
- **2013**: Fabrication of planar heterojunction perovskite solar cells by Snaith *et al.*,[f] achieving a PCE of 15.4%.
- **Today - 2024**: The record for perovskite solar cells (single junction) currently lies at 26.7%, at the level of silicon solar cells. Halide perovskites are also explored for other technologies.

[a] Mitzi, D. B., *et al.* (1994). *Nature*, 369(6480), 467-469.
[b] Chondroudis, K., & Mitzi, D. B. (1999). *Chemistry of materials*, 11(11), 3028-3030.
[c] Kojima, A., *et al.* (2009). *Journal of the american chemical society*, 131(17), 6050-6051.
[d] Kim, H. S., *et al.* (2012). *Scientific reports*, 2(1), 591.
[e] Lee, M. M., *et al.* (2012). *Science*, 338(6107), 643-647.
[f] Liu, M., *et al.* (2013). *Nature*, 501(7467), 395-398.

Questions

Note that some questions relate to previous sections of the MRes course.

- Can you guess the oxidation states in the perovskite oxide $KTaO_3$?
- Can you demonstrate the relation for the Goldschmidt Tolerance Factor? (Using simple geometry)
- From what you have seen so far about organic semiconductors and halide perovskites, how do you think the dispersion relation compares between these two families of materials?

- Where do you think defects come from in perovskites? (We will see this in more details in Lecture 4.)
- If ionic motion screens the internal electric field in the perovskite layer, what mechanism ensures extraction of carriers in perovskite solar cells?
- Write down the oxidation state of each element in the chemical formula of 2D perovskites (section 1.3). Verify that charge neutrality is ensured.

Sources used in this Lecture

- Frost, J.M., Walsh, A. (2016). Molecular Motion and Dynamic Crystal Structures of Hybrid Halide Perovskites. Chapter 1 in: Park, NG., Grätzel, M., Miyasaka, T. (eds) Organic-Inorganic Halide Perovskite Photovoltaics. Springer, Cham.
- Wei, L., Stroppa, A., Wang, Z. M., & Gao, S. (2020). Hybrid organic-inorganic perovskites. John Wiley & Sons. (Chapter 1: Introduction to Hybrid Organic-Inorganic Perovskites)
- Yin, W. J., Yang, J. H., Kang, J., Yan, Y., & Wei, S. H. (2015). Halide perovskite materials for solar cells: a theoretical review. *Journal of Materials Chemistry A*, 3(17), 8926-8942.

Lecture 2: Halide perovskite thin film formation

Introduction

The 'soft' nature of halide perovskites enables the use of low-temperature fabrication methods and provides opportunities to manipulate film formation. In this lecture we will explore the fundamentals of perovskte film growth. Note that we will not cover single crystal synthesis, which is also explored for perovskite-based devices. In Lecture 3 we will cover the basic material and optical characterisation techniques to assess the quality and morphology of your film. These two lectures combined will allow you to: 1) design an experimental plan to grow perovskte thin films, 2) verify the quality of your film, and 3) gather initial information on your perovskite.

Contents

Why do we care?

Mixing precursors into a solvent and obtaining a film from spincoating is easy. But how good is your film? What makes a good film? And how can you control its quality during the processing steps? Considering and answering these fundamental questions will lay the foundations for good research practices and critical thinking.

1 Thin film formation

1.1 Nucleation

The **nucleation** step in thin film formation dictates the nature of the subsequent growth processes and, therefore, the final film morphology. When depositing the precursors in solution phase (more details in section 2.1), the first step consists in solvent removal inducing an increase in precursor concentration towards or beyond saturation. This saturation of the precursors results in the formation of molecules of the nucleating phase, which cluster together into single-crystal nuclei. Nuclei form at the substrate-solution interface and/or within the precursor solution (Fig. 2.1a). The former and latter mechanisms are referred to as heterogeneous and homogeneous nucleation, respectively.

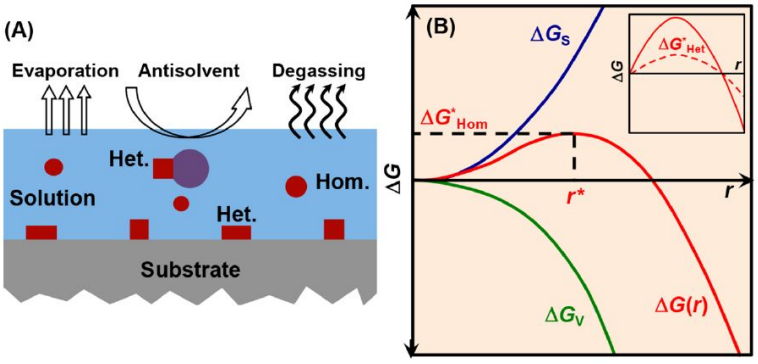

Figure 2.1: (a) Schematic illustration of homogeneous and heterogeneous nucleation during supersaturation. (b) Evolutions of total free energy change ΔG, surface ΔG_S and volume ΔG_V free energy changes as a function of nucleus radius r for homogeneous nucleation (inset: heterogeneous nucleation).[1]

The ability of a dissolved substance to nucleate is described in thermodynamics using the **Gibbs free energy** change ΔG of the system. In this context, ΔG can be interpreted as the energy required for

[1] Zhou, Y., *et al.*. (2015). *The journal of physical chemistry letters*, 6(23), 4827-4839.

nucleation to take place. In the case of homogeneous nucleation, the total free energy change ΔG is related to the radius of the nucleus r by:

$$\Delta G(r) = -V(r)\Delta g_V + A(r)\gamma_{CL}, \tag{2.1}$$

where $V(r)$ and $A(r)$ are the volume and area of the nucleus, Δg_V is the difference in free energy per unit volume between the phase that nucleates and the thermodynamic phase the nucleation is occurring in, and γ_{CL} is the surface tension of the interface between the liquid and the crystalline nucleus. Therefore, ΔG evolves with the radius of the nucleus r according to:

$$\Delta G(r) = -\left(\frac{4}{3}\pi r^3\right)\Delta g_V + 4\pi r^2 \gamma_{CL}. \tag{2.2}$$

Fig. 2.1b represents the evolution of total free energy change ΔG, which is a sum of the free energy change associated with the creation of nucleus/solution interface ($\Delta G_S > 0$, unfavourable) and the free energy change associated with the conversion of a volume of precursor solution to crystalline nucleus ($\Delta G_V < 0$, favourable). The maximum ΔG^*_{Hom} occurs at the critical nucleus radius r^*. Nuclei with $r > r^*$ are thermodynamically stable and will trigger **crystal growth**.

The size distribution of the nuclei plays an important role in the final microstructure of the film. To achieve a high density of nuclei uniform in size, crystallisation should occur through rapid saturation of the precursors. Once stable nuclei are formed, crystal growth takes place to reduce the overall free energy. The precursor concentration must remain above the solubility limit to ensure continuous growth.

1.2 Growth

There are three major mechanisms by which nuclei growth can occur (Fig. 2.2):

- **Island growth - Volmer-Weber**: Nuclei grow both vertically and laterally via attachments of 'monomers'. In this case, bonding between the 'monomers' and the growing phase is much stronger than between the 'monomers' and the substrate. A dense polycrystalline film forms as the islands coalesce, provided that sufficient precursors remain available.
- **Layer growth - Frank-van der Merwe**: Layer growth mode occurs when bonding between the 'monomers' and the substrate is stronger than between 'monomers'.
- **Layer-island growth - Stranski-Krastanov**: The intermediate layer-island growth mode is most appropriate to describe thin film perovskite growth.

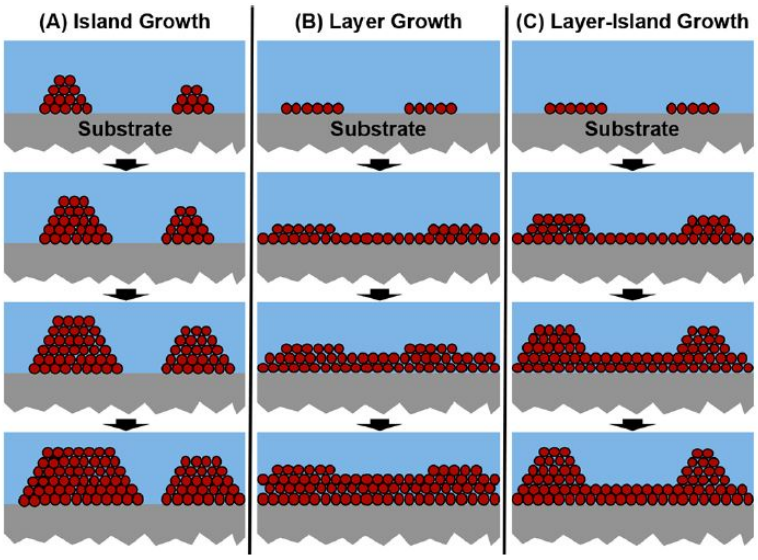

Figure 2.2: Illustration of the three major growth mechanisms: (a) island growth, (b) layer growth, and (c) layer-island growth.[2]

[2]Dunlap-Shohl, W. A., *et al.* (2018). *Chemical reviews*, 119(5), 3193-3295.

2 Thin film processing

A wide range of deposition techniques are explored to grow high quality perovskite thin films, and can be divided in two categories:

- Deposition from solution
- Deposition from vapour phase

In this lecture, we focus on the major processing techniques used to grow perovskite thin films in each category: **spincoating** and **thermal evaporation** (see Fig. 2.3). Regardless of the deposition technique, the goal is to obtain a well-ordered film with good coverage through dense, free of pinholes, and uniform nucleation of the perovskite grains.

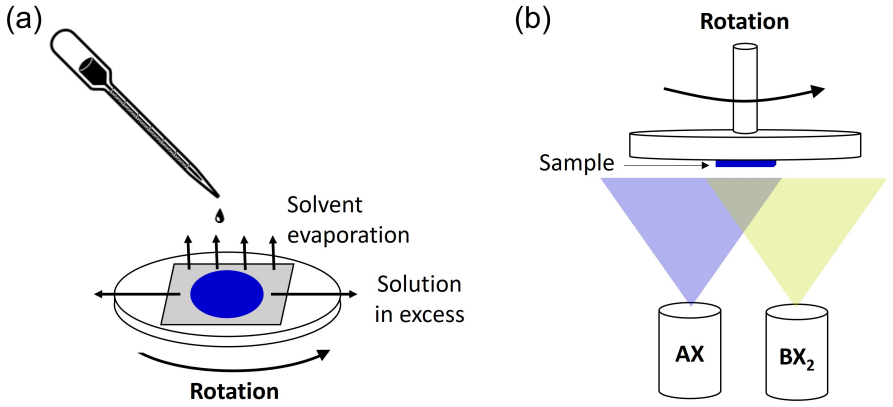

Figure 2.3: Illustration of spincoating (a) and thermal evaporation (b) deposition technique.

2.1 Spincoating

When growing perovskite films from the solution, variables available for **microstructure** tuning include solvents, additives (e.g., thiocyanate-based salts), antisolvent, temperature, atmosphere, and time. **Polar aprotic** (lacks an acidic proton) **solvents** such as dimethylformamide (DMF) and dimethyl sulfoxide (DMSO) are used for their particular ability to dissolve salts. In the one-step deposition method, all **precursors** (e.g., MAI and PbI_2) are mixed in a solvent or solvent mixture. This solution is dropped on a substrate and a spincoating step ensures homogeneous spreading of the solution and evaporation of the solvent. As the solvent evaporates, the concentration of the precursors increases until it reaches the solubility limit (supersaturation), triggering nucleation and growth of the perovskite phase.

A solid **intermediate phase** may form during the growth process with these solvents. The most encountered intermediates include adducts and complexes such as PbI_2·nDMSO and MAI·PbI_2·DMF. The formation of appropriate intermediate phases can favour homogeneous and dense crystal growth. Nevertheless, the persistence of these phases in the final film should be avoided and can be probed using X-ray diffraction (XRD) (see Lecture 3).

To accelerate the removal of solvent and the supersaturation of the precursors, a technique known as '**antisolvent washing**' is used during the spincoating step. A **nonpolar antisolvent** (e.g., toluene, or chlorobenzene) is dripped on the substrate and mixes with the polar solvent, driving the solvent out faster than it would through evaporation. As nonpolar solvents do not dissolve halide salts, antisolvent dripping reduces the precursor solubility in the remaining solution resulting in a reduction of the critical radius r^* for nucleation. This drives a rapid 'burst' of nucleation and results in high nucleation density to obtain a uniform, compact, and pinhole-free microstructure. Yet, a precise time must be chosen to drip the antisolvent and trigger the washing process, making this processing technique challenging for large-scale use.

2.2 Thermal evaporation

Perovskite films processed by thermal evaporation rely on **coevaporation** in vacuum of all precursors. The mixture of vapours condenses on the substrate to form a film. Perovskite-phase formation is achieved through substrate-dependent chemical reactions. Yet, amorphous films (<100 nm grains) are generally obtained from thermal evaporation, and post-deposition treatments such as thermal annealing are necessary to initiate crystal growth and large grain formation (see section 3). Thermal evaporation requires optimisation of precursor evaporation rates to achieve the targeted stoichiometry (e.g., ABX_3) and prevent formation of secondary phases, which can be controlled using XRD (see Lecture 3).

Note that both processing techniques are described for the 'one-step' deposition method, where all precursors are mixed (in solution) or evaporated simultaneously. 'Two-step' deposition is also possible in both solution and vapour phase methods with successive deposition of the precursors. The second step of the deposition generally triggers the reaction for perovskite phase formation.

3 Post-deposition treatment

Post-deposition treatments are considered to 1) remove remaining solvent (in case of solution processing), 2) convert intermediate phases to the perovskite phase, 3) assist in the growth of the film, and 4) coarsen the grains. **Thermal annealing** is a standard post-deposition treatment generally conducted at moderate temperature (generally $\sim$100°C) for hybrid organic-inorganic halide perovskites. The ability to improve the morphology of a film at relatively low temperature is a feature attributed to the soft nature of halide perovskites. Yet, the annealing treatment is also constrained by an upper limit on temperature to avoid perovskite decomposition, change in the film stoichiometry and defect formation.

Thermal annealing is particularly important for perovskite films obtained from the vapour phase to ensure grain growth, which can be monitored by Scanning Electron Microscope (SEM) (see Lecture 3). When elevated temperatures are required to achieve large and ordered grains, annealing in precursor vapor or pressurised environment should be considered to prevent loss of the most volatile precursor.

Now that you have processed your perovskite film, how do you characterise it?

Questions

- How do you think the substrate can impact nucleation and crystal growth?
- You want to prepare a precursor solution for $MAPbI_3$ formation with a precursor concentration of 1 $mol.L^{-1}$. What masses of precursors do you need to dissolve in 1 mL of solvent?
- What do you think happens if you drop the antisolvent too early or too late in the spincoating step?
- Your goal is to grow $CsPbBr_3$ films by thermal evaporation. For your first attempt you use evaporation rates of 1 Å/s for both CsBr and $PbBr_2$ precursors, followed by a thermal annealing treatment. Subsequent characterisation of your film reveals a secondary phase of CsBr. How can you adapt you deposition process?

Sources used in this Lecture

- Dunlap-Shohl, W. A., Zhou, Y., Padture, N., & Mitzi, D. B. (2018). Synthetic Approached for Halide Perovskite Thin Films. *Chemical Reviews*, 119(5), 3193-3295.

Lecture 3: Halide perovskite thin film characterisation

Introduction

Now that you have processed your perovskite film, how do you characterise it? In this lecture we will explore the basic material and optical characterisation techniques that allow you to verify the quality of your film, and gather initial information on your perovskite. Going through these characterisations carefully can be crucial to avoid misinterpretations in further research.

Contents

Why do we care?

Mixing precursors into a solvent and obtaining a film from spincoating is easy. But how good is your film? What makes a good film? And how can you control its quality during the processing steps? Considering and answering these fundamental questions will lay the foundations for good research practices and critical thinking.

1 Material characterisation

Key questions to answer about the microstructure of your film are:

- Have I formed the perovskite phase targeted?
- Are there secondary phases remaining in the film?
- What is the nature and level of crystalline order in my film?
- Is my film continuous, homogenous, and compact?

1.1 Crystal structure

X-ray diffraction (XRD) is widely used to probe the microsctruture of perovskite films including phase identification and quantification, texture analysis, microstrain, and macrostrain. The box at the end of this section is a reminder of the basics of X-ray diffraction.

Fig. 3.1 displays a calculated XRD pattern for $MAPbI_3$ in its cubic phase. The first three peaks correspond to the (100), (110), and (111) crystal planes. Simulated XRD patterns are particularly useful for the analysis of XRD data, containing information on peak position and relative intensity. Such simulations can be done through softwares such as Mercury using crystallographic information file (*.cif) as input. Comparing measured with simulated XRD patterns enables to:

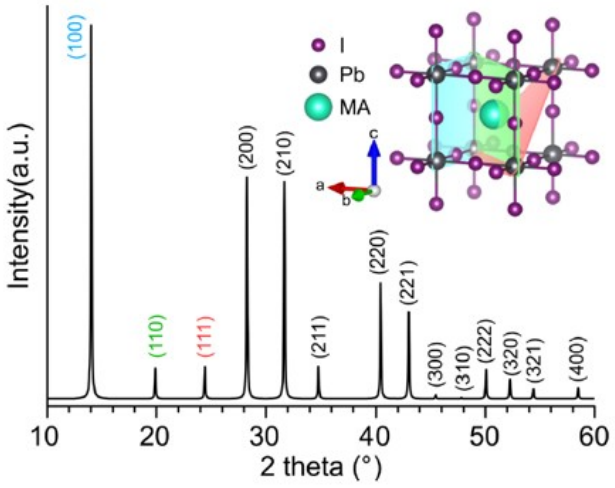

Figure 3.1: Simulated XRD pattern of $MAPbI_3$ in its cubic phase. The inset displays the corresponding crystal structures with (100), (110), and (111) crystal planes.[1]

[1] Tan, W. L., & McNeill, C. R. (2022). *Applied Physics Reviews*, 9(2).

- Identify the crystal phase of the perovskites (e.g., cubic, tetragonal, or orthorhombic for $MAPbI_3$).
- Index peaks and identify potential **preferred orientations**.
- Identify crystalline secondary phases.

The ability to fit a specific crystalline structure to an XRD pattern using appropriate softwares provides a wealth of information including unit cell parameter, crystallite orientation, and quantity of various phases. Moreover, microstructural information such as crystallite size and microstrain can be inferred from the width and shape of the diffraction peaks. More advanced X-rays based techniques including grazing-incidence wide-angle X-ray scattering (GIWAXS) at synchrotron facilities can provide further microstructural information and allows for in-situ and in-operando measurements for probing the evolution of crystal phase in real time during crystal growth or solar cell operation.

X-Ray diffraction (XRD)

Bragg's law lays the foundation of XRD. In a crystalline material, the periodic arrangement of atoms results in constructive and destructive interference of X-rays. Constructive interference of X-rays can occur as their wavelength is comparable to atomic spacing and can therefore satisfy Bragg's law:

$$2dsin\theta = n\lambda, \tag{3.1}$$

with d the distance between atomic planes, θ the angle of incident X-rays, n an integer corresponding to the order of reflection, and λ the wavelength of the X-rays. Constructive interference takes place when the phase shift between diffracted X-rays is an integer multiple of the wavelength (Fig. 3.2). A typical **XRD pattern** is collected as a function of 2θ. Diffraction peaks are indexed to an (hkl) **Miller index** representing the crystal plane intersecting the three crystallographic axes at a distance $1/h$, $1/k$, and $1/l$ along the corresponding lattice vector.

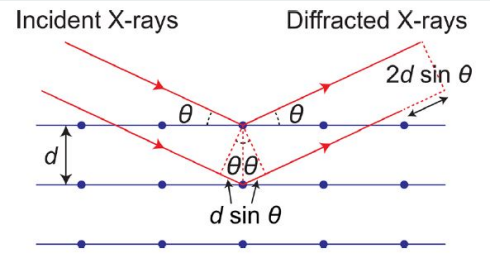

Figure 3.2: Schematic diagram showing the Bragg diffraction of X-rays from atomic planes of a crystalline materials with interplanar distance d.[2]

[2] Tan, W. L., & McNeill, C. R. (2022). *Applied Physics Reviews*, 9(2).

1.2 Film morphology

When optimising a thin film for devices fabrication, morphological aspects must be considered:

- *Coverage*: Full coverage with the absence of pinholes is a key prerequisite to prevent the formation of shunt paths leading to leakage current in vertical devices.
- *Surface roughness*: Rough films may cause issues when they prevent conformal deposition of overlying layers in the device.
- *Grain boundaries*: As grain boundaries can induce energy barriers and charge scattering, it is usually considered desirable to have larger grains. In particular, grains extending across the full film thickness in vertical devices is targeted (for vertical devices). Moreover, grain boundaries can serve as 'highways' for detrimental transport of ions, oxygen, and moisture. Larger grain sizes implying a lower grain boundary density is often desired to improve the stability of the device. Yet, a trade-off in grain size must generally be met to prevent pinhole formation (point 1).
- *Intra-grain microstructure*: Defects in intra-grain regions may be generated by sub-grain domain formation, stacking faults, and dislocations.
- *Heterogeneous phases/composition*: Phase segregation or the persistence of secondary phases in the final film can be unintentional and harmful, or intentionally targeted to tune optoelectronic properties.

Mapping these phases can be key in the understanding of the perovskite film properties.

Scanning electron microscopy (SEM) is an ideal characterisation tool to investigate these various aspects of the film morphology (Fig. 3.3). **Secondary (SE)** and **backscattered (BSE)** electrons signals complement each other to provide information on the film topography and inhomogeneities in composition. SEM can be complemented with **energy dispersive spectroscopy (EDS)** to identify the atomic number of atoms encountered. Intra-grain microsctructure is however difficult to infer from SEM and more advanced techniques such as **transmission electron microscopy (TEM)** must be used to access atomic-scale microstructure such as lattice spacings and structural imperfections (e.g., dislocation, stacking faults). **Atomic force miscoscopy (AFM)** may be used as an alternative technique, sometimes more easily accessible, to assess the morphology and surface roughness of the film.

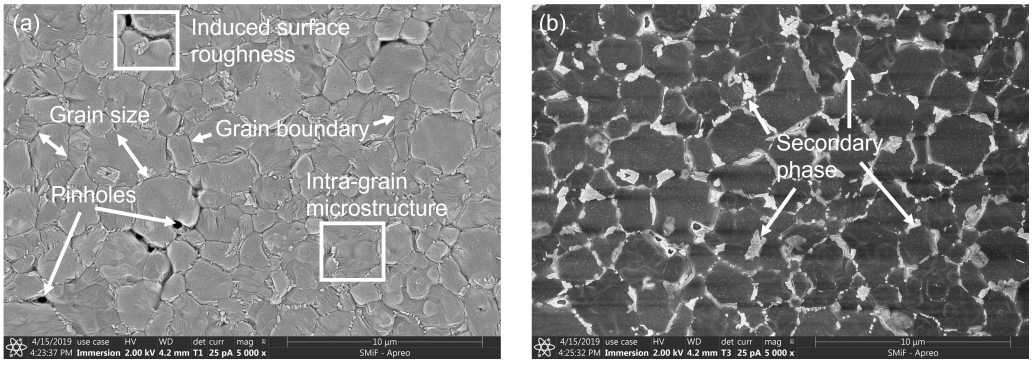

Figure 3.3: Scanning electron microscope images in secondary (a) and backscattered (b) electron mode for $MAPbI_3$ processed with 5% extra PbI_2. The secondary phase formed has been identified as PbI_2 from EDX and XRD measurements.

Scanning Electron Microscopy (SEM)

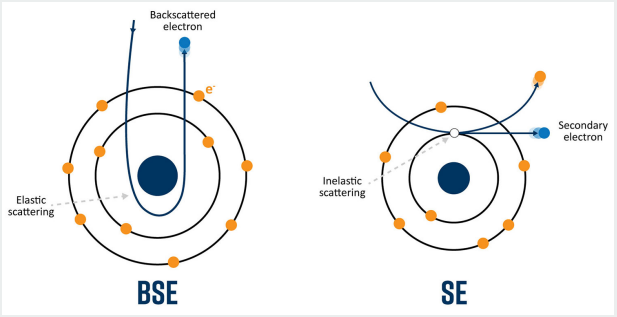

Figure 3.4: Schematic diagram of backscattered and secondary electrons generation.(https://www.nanoscience.com/techniques/scanning-electron-microscopy/)

A **scanning electron microscope (SEM)** image is constructed from the interaction of an electron beam of energy between 0.1 and 50 kV with the sample. The output signal mainly consists of **secondary (SE)** and **backscattered electrons (BSE)**. SE are generated by **inelastic** collisions that excite electrons in the material and provide them with enough energy to escape. As only electrons within a few nm from the film surface are able to escape, the SE signal is particularly appropriate for an analysis of the film topography with high resolution (1-10 nm). BSE originate from **elastic** interactions between the electron beam and the sample. The reflected electrons can escape from a greater depth than SE as they have much high energy and are less influenced by scattering process on their way out of the sample. While BSE signal is usually of lower resolution than SE, it allows for mapping compositional differences as atoms with greater atomic number backscatter electrons with more energy.

2 Optical characterisation

Basic optical scectroscopy techniques can be used to access fundamental semiconductor properties such as bandgap, and more advanced information on charge carrier recombination. I will not present spectroscopy techniques in too much details here as this subject is covered more extensively by other lecturers in the programme.

2.1 Absorption

UV-vis-NIR absorption spectroscopy is a standard and widely available technique to characterise the optical properties of materials in solution or thin film. Absorption spectra can be used to 1) check the identity of your perovskite phase (if the spectrum is known), 2) extract the bandgap, and 3) extract information on excitonic properties (particularly relevant for layered perovskites). The **Tauc plot** is a method originally developed to extract the **optical gap** E_{opt} of amorphous inorganic semiconductors such as silicon and germanium (Fig. 3.5). It relies on the assumption of parabolic density of states distributions and can be used with both direct and indirect bandgap materials. This results in expressions describing the dependence of the absorption coefficient α with photon energy $h\nu$ near the band edge:

$$\alpha h\nu \propto (h\nu - E_{opt})^2 \tag{3.2}$$

for an **indirect** allowed interband transition, and

$$\alpha h\nu \propto (h\nu - E_{opt})^{1/2} \tag{3.3}$$

for a **direct** allowed interband transition. Therefore, plotting $(\alpha h\nu)^{1/2}$ and $(\alpha h\nu)^2$ as a function of $h\nu$ enables to determine the nature of the gap, direct or indirect, and the optical bandgap E_{opt}.

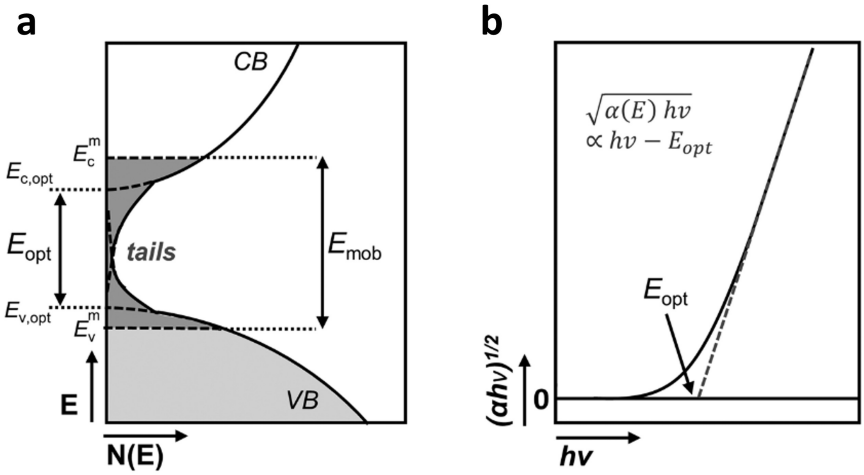

Figure 3.5: Typical density of states $N(E)$ as a function of energy E (a) and Tauc plot with optical bandgap E_{opt} extraction (b) for amorphous bulk 3D semiconductor.[3]CB and VB stand for conduction and valence bands. E_{mob} corresponds to the mobility gap between E_C^m and E_C^m, concept not covered in this lecture. α, h and ν correspond to the absorption coefficient, the Planck constant, and the photon frequency, respectively.

The Tauc plot analysis must however be considered with care when used on new materials as underlying assumptions may not be verified. For example, the Tauc analysis neglects the presence of strong excitonic interactions, which are typically observed in layered perovskites. **Elliott's theory** must be preferred to account for such excitonic states.

2.2 Photoluminescence

Steady-state and **time-resolved photoluminescence (PL and TRPL)** form another set of widely available optical characterisation techniques. Photoluminescence measurements probe the **radiative recombination** processes upon light excitation. Radiative recombination is the inverse process of absorption of photons and subsequent creation of electron-hole pairs. Photoluminescence spectroscopy measures the photoluminescence intensity as a function of emitted wavelength λ_{em} for a constant illumination with excitation wavelength λ_{exc}. TRPL spectroscopy resolves fast radiation processes occurring over a very short time scale (from ms to ps). A short and high energy pulse is used to detect the PL time dependence.

Comparison of steady-state PL spectra between different samples can provide information on the extent of **non-radiative recombination** and, therefore, the impact of defects in the bulk, at grain boundaries, or

[3]Klein, J., *et al.* (2023). *Advanced Functional Materials*, 2304523.

at interfaces with other layers. Nevertheless, the instability of halide perovskites to high light intensities make PL measurements and their interpretation challenging for this family of materials. It is for example common to observe the PL decreasing over successive measurements on a same spot. Care must therefore be taken when comparing the absolute intensity of perovskite PL spectra. The position of the PL emission peak can also be compared to the absorption edge to deduce the extent of **Stokes shift**, a measure of energy loss due to vibrational relaxation and dissipation. 3D Pb-based halide perovskites typically exhibit almost nonexistent Stokes shift. A larger Stokes shift can however be measured in lower dimensional perovskites, and in particular perovskite quantum dots, a phenomenon that can be leveraged in medical imaging applications.

TRPL is a standard tool to access the minority **carrier recombination lifetime** τ. Nevertheless, a wide range of values between the ns and µs range have been measured. This lack of consistency is partly due to reproducibility issues in perovskite film processing, and partly to the strong influence of light intensity on recombination mechanisms. In particular, a bimolecular recombination regime is typically reached at fluences used in TRPL measurements. In this regime, the measured recombination lifetime decreases with increasing light intensity, making any extraction strongly light-intensity sensitive.

With the use of these basic material and optical characterisation techniques, you can establish some important background knowledge about your film including the phase obtained, the morphology, and information on recombination of charge carriers.

Questions

- Check out the XRD pattern of $MAPbI_3$ on Mercury. Mercury can be downloaded for free on the CCDC website. The *.cif file for $MAPbI_3$ is available on Blackboard.
- What would you expect to happen to the width of diffraction peaks as grain size decreases and disorder increases?
- In Fig. 3.3b, the two phases identified are $MAPbI_3$ and PbI_2. Which phase appears with the lighter colour? Why?
- What do you think a PL spectrum would look like with a mixture of the two perovskites $MAPbI_3$ and $MAPbBr_3$? How could you use photoluminescence to determine if iodine and bromine atoms are homogeneously distributed in a film of mixed halide perovskite $MAPbI_xBr_{3-x}$?

Sources used in this Lecture

- Tan, W. L., & McNeill, C. R. (2022). X-ray diffraction of photovoltaic perovskites: Principles and applications. *Applied Physics Reviews*, 9, 021310.
- Klein, J., Kampermann, L., Mockenhaupt, B., Behrens, M., Strunk, J., & Bacher, G. (2023). Limitations of the Tauc Plot Method. *Advanced Functional Materials*, 2304523.

Lecture 4: Mastering defects in halide perovskites

Introduction

All semiconductors outside a computer simulation contain defects. The microelectronic industry has thrived as a result of very advanced processing technologies allowing for defect control. While some defects must be avoided (e.g., stalking faults, grain boundaries, dangling bonds...), others can be intentionally engineered to enable electronic and optical features (e.g., electrical doping, colour centres...). Due to strong covalent bonding, defect engineering and control in traditional inorganic semiconductors (e.g., silicon) require advanced, energy-intensive and expensive processing tools (wafer growth, ion implantation...). The softer chemical bonds (ionic and Van der Waals) of emerging electronic materials, including organic semiconductors and halide perovskites, offers two major advantages: 1) low temperature and less energy-intensive processing techniques (Lecture 2), and 2) a reduced impact of defects on optoelectronic properties (Lecture 4). Yet, this softness is inevitably associated with important drawbacks including a low level of order (organic semiconductor lectures), and a challenging use of defects to tune optoelectronic properties (e.g., doping - Lecture 4). In this lecture, we will cover the basics of semiconductor defects before exploring the peculiarities of halide perovskite defects.

Contents

Why do we care?

You have fabricated a device, say a solar cell. Your figures of merit tell you you have achieved a certain efficiency. Now what? Defects are very often the culprit in low device efficiency. But if we want to fix them, or engineer them, we need to go to the source.
What are the sources of defects? What is their impact on optoelectronic properties?

1 Defects in semiconductors - The basics

1.1 Defect chemistry

Fig. 4.1 summarizes the various types of crystallographic defects. There are two major ways to categorize defects. The first one consists in differentiating the origin of the defects: **intrinsic** (b-f, i-k) vs **extrinsic** (g-h). Interruptions in the crystal lattice are intrinsic to the material and generally detrimental to device performance. The addition of impurities in the crystal lattice can be detrimental (when unintentional) or provide specific optoelectronic properties (e.g., dopant impurities).

One can also differentiate the extent of the defect: **point defect** (b-h) vs **higher dimension defects** (i-k). Higher dimension defects include edge dislocations (i), grain boundaries (j), and precipitates or phase segregation (k). Point defects can take the form of **vacancies** (atoms missing from their lattice site: b), **interstitials** (atoms occupying empty space between lattice sites: c, h), and **substitutionals** (atoms occupying another lattice site: d, g). The Kröger-Vink notation is used to describe point defects in crystals: A_B where A is the species of interest and B the lattice site occupied by the species. For example, V_{Pb} is

a vacancy of the Pb site, Pb_i an interstitial of Pb, and I_{Pb} an I atom occupying a Pb site (Pb substituted by I).

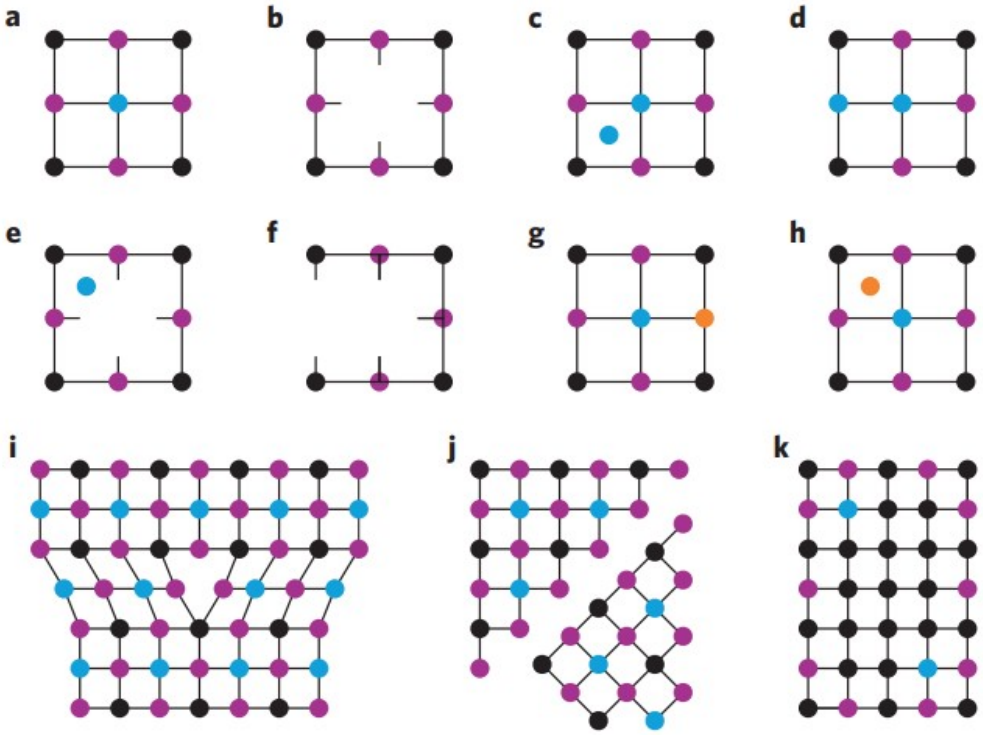

Figure 4.1: Illustration of defects in a crystal containing three elements (black, purple, and blue). a) Perfect lattice. b) Vacancy. c) Interstitial. d) Substitution. e) Frenkel defect (interstitial and vacancy created from the same ion). f) Schottky defect (anion and cation vacancies occurring together). g) Substitutional impurity. h) Interstitial impurity. i) Edge dislocation (line defect propagating along the axis perpendicular to the page). j) Grain boundary. k) Precipitate.[1]

Point defects can be charged. To maintain charge neutrality, defects generally appear in pairs of opposite charge. **Frenkel defects** are obtained when two defects with the same ion are formed (e). A pair of defects from two different ions is called **Schottky defect** (f).

A defect will form in a crystal lattice when it is thermodynamically favourable. The **formation energy** ΔH for a defect α ionized to the charge state q is given by:

$$\Delta H^{(\alpha,q)}\left(\mu_i, E_F\right) = \Delta H^{(\alpha,q)}\left(0,0\right) + \sum_i n_i\mu_i + qE_F \tag{4.1}$$

where $\sum_i n_i\mu_i$ is the sum of the **chemical potentials** μ of the constituent elements i (with n_i the number of element i), $\Delta H^{(\alpha,q)}\left(0,0\right)$ is the defect formation energy for $\mu_i = 0$ and $E_F = 0$, with E_F the Fermi energy referenced to the valence band maximum. The chemical potentials μ_i are directly influenced by the crystal growth conditions. A defect with negative formation energy $\Delta H < 0$ will form spontaneously (thermodynamically favourable). We can see in equation 4.1 that the formation energy also depends on the Fermi energy position.

To summarise equation 4.1:

- The likelihood of a defect to form will depend on the growth conditions (solvent, atmosphere, temperature, stoichiometry of precursors, additives...).
- Competition between defect formation will determine the position of the Fermi level in the bandgap.

[1] Ball, J. M., and Petrozza, A. (2016). *Nature Energy*, 1(11), 16149.

1.2 Impact on optoelectronic properties

Defects are modeled with energy levels in the energy band diagram. The position of the energy level is determined by the transition energy required for a defect to change oxidation state. Defects with energy levels falling within the bandgap of a semiconductor will impact optoelectronic properties. Fig. 4.2 illustrates how charge carriers (electrons and holes) can interact with energy levels situated in the bandgap.

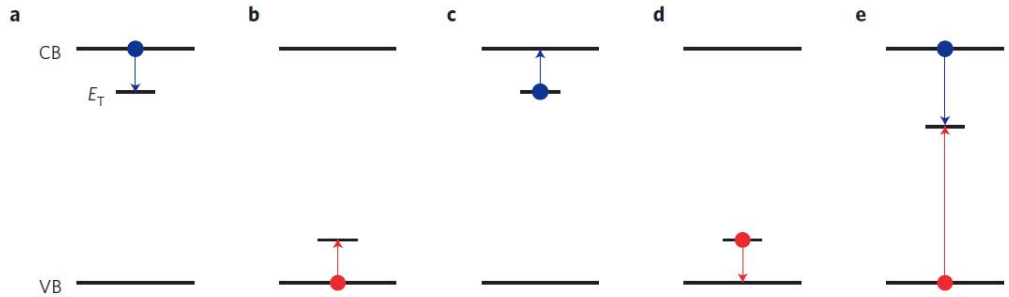

Figure 4.2: Schematic view of the interaction of charge carriers (electrons in blue and holes in red) with defects (traps). a) Electron capture (trapping) by a defect of energy E_T between the conduction band (CB) and valence band (VB). The arrow indicates the direction of the transition. b) Hole capture. c) Electron emission (de-trapping or doping). d) Hole emission. e) Hole-electron recombination through capture in the same trap.[2]

Defects can be differentiated according to the position of their energy level within the bandgap: **shallow traps** exhibit energy levels close to (within a few k_BT, with k_B the Boltzmann constant and T the temperature) the conduction or valence band (a-d), while **deep traps** are typically associated with energy levels situated close to the middle of the gap (e). As a consequence, shallow traps will impact charge transport through trapping-detrapping process, while deep traps lead to charge recombination. Deep traps are particularly harmful for optoelectronic devices such as solar cells.

As stated earlier, defects can also be intentionally engineered to fulfill specific optoelectronic features, with **doping** being the most common one. Electrical doping (see section 3) aims at tuning the density of free holes and electrons in a semiconductor. **p-type** semiconductors exhibit and excess of holes (E_F closer to the valence band), and **n-type** semiconductors an excess of electrons (E_F closer to the conduction band). Dopant engineering therefore requires a transition level of the defect close to the targeted band to enable efficient ionization and emission of a free carrier.

Traps are also categorized by their propensity to emit/trap positive or negative charge carriers and change oxidation state. **Donor** levels donate electrons and **acceptor** levels accept electrons. Therefore, a donor level close to the conduction band will act as an n-type dopant, while a donor level close to the valence band will act as hole trap (traps a hole and donate an electron to the valence band). Following the same logic, acceptor levels close to the conduction band will act as electron trap, while acceptor levels close to the valence band act as hole dopant (accept an electron from the valence band leaving an extra hole behind).

Now, what about defects in halide perovskites?

2 Defect formation in halide perovskites

Density Functional Theory (DFT) is a powerful tool to determine via calculations what defects are the most likely to form (formation energy), what energy level they would take (transition energy), and how these defects will position the Fermi level.

[2] Ball, J. M., and Petrozza, A. (2016). *Nature Energy*, 1(11), 16149.

2.1 Transition energy

As a first step, we want to determine the **transition energies** for typical intrinsic defects in a given halide perovskite. The transition level of a defect is the Fermi level position where the defect can donate/accept electrons. We focus here on $MAPbI_3$. Examples of intrinsic defects in this perovskite would be Pb vacancy (V_{Pb}), I interstitial (I_i), or Pb substituted by MA (MA_{Pb}).

Fig. 4.3, taken from the literature,[3] summarises the transition energies of all possible intrinsic point defects in $MAPbI_3$. With a transition energy corresponding to an oxidation of the defect (e.g., $0/+1$), the trap is considered a donor level (the defects donates an electron and becomes more positively ionised). Similarly, transition energies associated with a reduction of the defect (e.g., 0/-1) correspond to acceptor levels (accepting electrons becoming more negatively ionised).

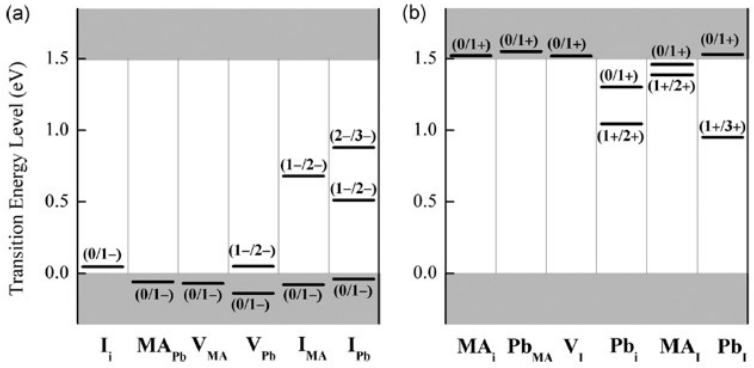

Figure 4.3: Transition energy levels of (a) intrinsic acceptors and (b) intrinsic donors in $MAPbI_3$ obtained from DFT calculations.[3]

Many intrinsic defects in $MAPbI_3$ have transition energies situated within the conduction/valence bands, and are therefore inactive. Within the bandgap, we can identify trap levels close to the conduction band minimum / valence band maximum, and deep in the bandgap. To determine potential harmful defects, their likelihood to form (formation energy) must be calculated.

2.2 Formation energy

The defect formation energy calculation (equation 4.1) depends on the chemical potentials of the crystal constituents. A first step is therefore necessary to determine the possible chemical potentials leading to the targeted phase of the perovskite, here $MAPbI_3$.

In thermodynamic equilibrium growth conditions, the existence of $MAPbI_3$ should satisfy:

$$\mu_{MA} + \mu_{Pb} + 3\mu_I = \Delta H\left(MAPbI_3\right), \tag{4.2}$$

where $\Delta H\left(MAPbI_3\right)$ is the formation enthalpy of $MAPbI_3$.

Additional constraints must be satisfied to exclude the formation of secondary phases (PbI_2 and MAI):

$$\mu_{MA} + \mu_I < \Delta H\left(MAI\right) \tag{4.3}$$

and

$$\mu_{Pb} + 2\mu_I < \Delta H\left(PbI_2\right). \tag{4.4}$$

Fig. 4.4 displays the calculated thermodynamic stable phases as a function of Pb and I chemical potentials (μ_{Pb} and μ_I). The chemical potentials of Pb and I satisfying equations 4.2 to 4.4 correspond to the red region. The narrowness of the thermodynamic stable range highlights that growth conditions should be carefully controlled to form the stoichiometry of $MAPbI_3$ perovskite phase. In the following, we choose to focus on three specific points (A, B and C) to look at calculated defect formation energies. Point B would correspond to

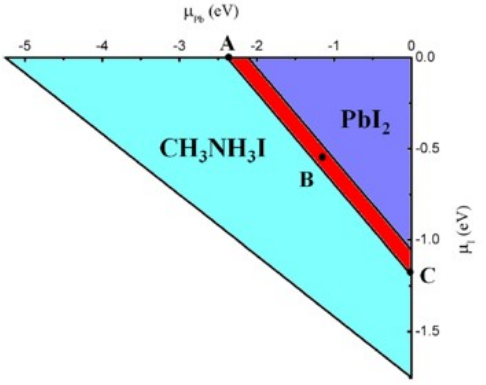

Figure 4.4: Thermodynamic stable phases for varying Pb and I chemical potentials. The specific points A, B, and C will be chosen to explore defect formation energies.[3]

[3]Yin, W.-J., Shi, T., and Yan, Y. (2014). *App. Phys. Lett.*, 104(6), 063903.

moderate growth condition, while points A and C are associated with I-rich/Pb-poor and I-poor/Pb-rich conditions, respectively. In practice, Pb-rich/I-poor condition is for example obtained by having a relatively higher proportion of PbI_2 than MAI in the precursor solution.

The defect formation energies calculated at different chemical potentials (different panels) and as a function of Fermi level are shown in Fig. 4.5. Formation energy graphs can appear daunting at first sight, but they contain key information on the electronic properties of your material:

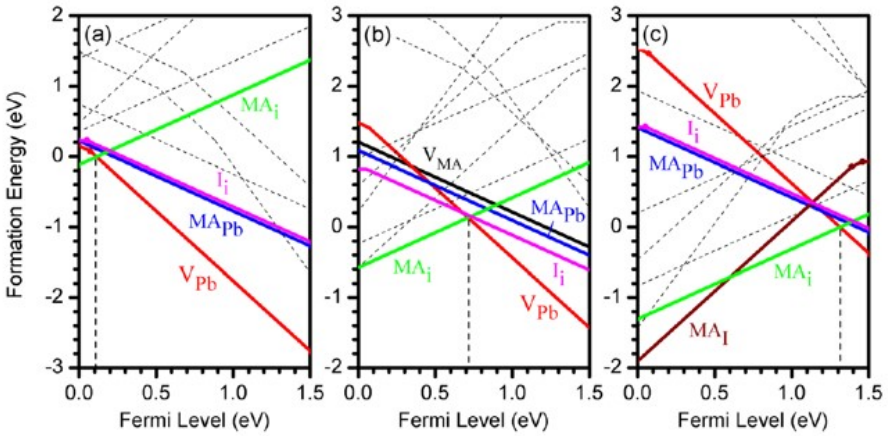

Figure 4.5: Formation energies of intrinsic point defects in $MAPbI_3$ calculated at chemical potentials A in panel (a), B in panel (b), and C in panel (c). The Fermi level is given with respect to the valence band maximum. Defects with lower formation energies (more likely to form) are displayed in color full lines, and defects with higher formation energies (less likely to form) are displayed in black dashed lines.[4]

- Different point defects have different formation energies. Defects with negative formation energies will form spontaneously. **Defects with the lowest formation energies will form in higher densities.** We are therefore only interested in the defect with the lowest formation energies displayed in colour in Fig. 4.5.

- As expected, **the formation energy is E_F-dependent**. The formation energy increases as the Fermi level increases (gets closer to the conduction band) for donor levels. In other words, the more n-doped the semiconductor becomes (E_F getting closer to CB), the less likely n-type dopant defect (donor levels) will form. Similarly, the formation energy increases as the Fermi level decreases (gets closer to the valence band) for acceptor levels.

- To understand how the Fermi level position is determined for a given growth condition, let's focus on panel (b). If E_F is close to the valence band, the most likely defects to form are MA_I, which are donor levels (see Fig. 4.3). Donor levels will tend to n-dope the semiconductor shifting E_F closer to the conduction band. When E_F get closer to the conduction band, the most likely defects to form are V_{Pb}, which are acceptor levels. These acceptor-type defects will tend to p-dope the semiconductor shifting back E_F closer to the valence band. **An equilibrium position is reach for E_F which depends on the relative formation energies of intrinsic point defects.** In moderate growth condition, $MAPbI_3$ is expected to be intrinsic as E_F is positioned close to the middle of the bandgap.

- Panel (a) and (c) highlight that **E_F can be shifted closer to the valence band (p-type doping) or conduction band (n-type doping) when growth conditions are varied**. In the I-rich/Pb-poor case (panel (a)), E_F is shifted closer to the valence band. In the I-poor/Pb-rich case (panel (c)), E_F is shifted closer to the conduction band. This principle has been explored as a doping strategy (see section 3.1).

- Another very important information to extract from formation energy calculations is the **propensity of the material to form deep and/or shallow defects**. In combination with Fig. 4.3, we can

[4]Yin, W.-J., Shi, T., and Yan, Y. (2014). *App. Phys. Lett.*, 104(6), 063903.

conclude that all defects with the lowest formation energies are shallow defects. Indeed, deep defects in $MAPbI_3$ have high formation energies and are unlikely to form.

2.3 Impact on optoelectronic properties

As a consequence of the typical defect chemistry in Pb-halide perovskites, the following statements are generally made:

- **Non-radiative recombination is low in Pb-halide perovskites** due to the high formation energy of deep defects. This feature makes Pb-halide perovskites particularly interesting for photovoltaic applications.
- **Pb-halide perovskites tend to be close to intrinsic semiconductors** with the Fermi level lying close to the middle of the bandgap for moderate growth condition. This behaviour is associated with defect compensation between donor and acceptor levels.
- **The position of the Fermi level is very dependent on the growth conditions** which must be carefully controlled to achieve high efficiency devices.

3 Application of defects: The case of electrical doping

Electrical doping is the introduction of an impurity or defect to generate free carriers and shift the Fermi level within the bandgap. Doping enables the formation of p–n junctions and can improve contact quality between the semiconductor and the electrodes. Here, we give a very brief overview of the use of defects to achieve controlled n-type and p-type doping in halide perovskites.

3.1 Intrinsic defect doping

As discussed in section 2.2, the position of the Fermi level of the bandgap is expected to be strongly dependent on intrinsic defects and, therefore, growth condition. The Fermi level is pinned by compensation among dominant donor and acceptor levels. Fig. 4.5 suggests that p-type and n-type doping should be achievable in I-rich/Pb-poor and I-poor/Pb-rich conditions, respectively.

In practice, various strategies have been developed to tune the chemical potential of the constituents, including:

- Changing the ratio of the precursors (e.g., MAI and PbI_2) in solution.
- Annealing the film to induce slight decomposition and loss of one constituent (e.g., MA).
- Annealing the film under a specific vapour to induce exccess of one consituent (e.g., halide).

Regardless of the strategy used, is is generally observed and expected that a Pb-halide perovskite film $APbX_3$ with AX in excess will be slightly more p-type, while a similar perovskite with PbX_2 in excess will be slightly more n-type (Fig. 4.6).

Nevertheless, numerous experimental studies have shown that **the extent of doping achievable through intrinsic defect engineering remains very limited!** Charge compensation through spontaneous formation of competing defects is believed to be the culprit.

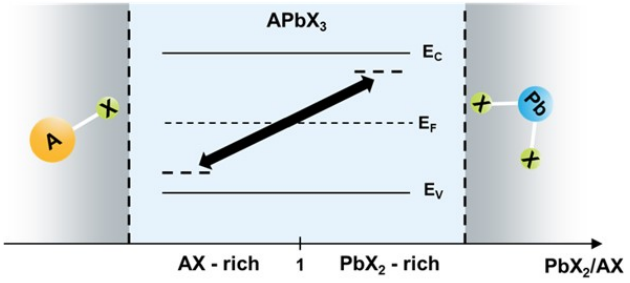

Figure 4.6: Schematic view of the Fermi level E_F evolution in $APbX_3$ perovskite structures, if the PbX_2/AX ratio is tuned from AX-rich to PbX_2-rich conditions. The existence of $APbX_3$ is constrained by the formation of secondary phases (AX and PbX_2).

3.2 Extrinsic defect doping

Traditional inorganic semiconductors like silicon are doped through the introduction of **impurity ions** in the crystal lattice. These substitutional defect impurities donate or accept an electron. A similar strategy has been explored for halide perovskites.

For an impurity dopant to successfully p- or n-dope a crystalline host, various criteria must be fulfilled such as:

- The defect formation must be thermodynamically favourable.
- The impurity ion must form the appropriate oxidation state to donate or accept an electron.
- The size of the impurity ion must be appropriate to form a substitutional or interstitial point defect.
- The transition energy of the defect formed enables efficient dopant ionisation at room temperature.

Experimental exploration of impurity dopants for halide perovskites can appear as difficult as finding a needle in a haystack, and DFT calculations prove crucial to accelerate the discovery process. As described in section 2, defect formation and transition energies can be calculated. Moreover, the formation energy of intrinsic defects will be strongly influenced by the formation of extrinsic defects, and their impact must be monitored.

Fig. 4.7 (a) displays the transition energies for potential impurity defects in $MAPbI_3$. According to this metric, many of them appear to be potential dopants with ionisation within a few k_BT. Fig. 4.7 (b) displays the formation energies for two selected defects, Sb_{Pb} and Bi_{Pb}, in addition to the dominant instrinsic defects (here MA_i, MA_I, and V_{Pb}). Both Sb_{Pb} and Bi_{Pb} are expected to be donor levels and therefore n-dope the perovskite host shifting the Fermi level towards the conduction band. Yet, in neither I-rich/Pb-poor or I-poor/Pb-rich conditions, these defects enable efficient n-type doping.

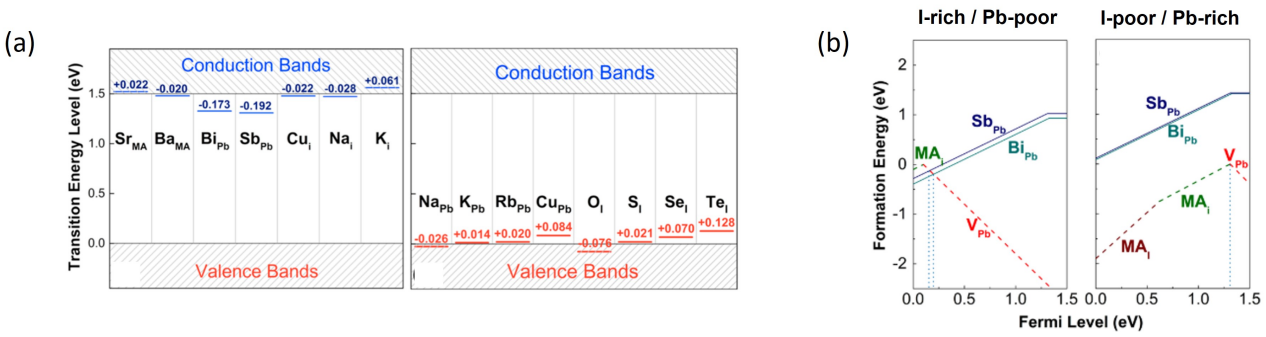

Figure 4.7: (a) Calculated transition energy levels of identified shallow donors (blue) and shallow acceptors (red) in $MAPbI_3$. (b) Calculated formation energies as a function of Fermi levels for Sb and Bi at I-rich/Pb-poor (left) and I-poor/Pb-rich (right) conditions.[5]

- In I-rich/Pb-poor condition: Formation of Sb_{Pb} and Bi_{Pb} are compensated by the concurrent increase in V_{Pb}, intrinsic acceptor-type defect. DFT calculations suggest that $MAPbI_3$ will remain p-type under this growth condition despite the introduction of n-type impurities.
- In I-poor/Pb-rich condition: The formation energies for Sb_{Pb} and Bi_{Pb} remain higher than for intrinsic defects. As a consequence, the Fermi level position remains pinned by intrinsic defects despite the the introduction of n-type impurities.

Overall, results suggest that **extrinsic defect doping in halide perovskites remains challenging as a consequence of charge compensation with intrinsic defects**.

[5]Shi, T., Yin, W.-J., and Yan, Y. (2014). *The Journal of Physical Chemistry C*, 118(44), 25350-25354.

3.3 Beyond point defect doping

In order to achieve efficient p- and n-type doping of halide perovskites, the research community is exploring strategies beyond point defect engineering. Charge transfer doping is used in organic semiconductors to promote free electrons/holes by mixing the semiconductor host with a donor/acceptor molecule. The use of this technique to dope halide perovskites has shown promising initial results.

Conclusion

This series of four lectures is intended to give an overview of the basics to better understand and undertake research in halide perovskites. For further information, you can refer to the sources listed at the end of each lecture.

Questions

Note that some questions relate to previous sections of the MRes course.

- If a Pb vacancy is formed in $MAPbI_3$, what other defect(s) could form to ensure charge neutrality in the solid? What could be an alternative to defect compensation?
- Thinking back to Lecture 3, how do you think high-dimensional defects such as grain boundaries could influence XRD patterns?
- Information on which type of defects would photoluminescence measurements provide?
- Considering that some defects have favourable formation energy at grain boundaries, what do you think happens locally to the Fermi level? Can you draw a band diagram showing the possible evolution(s) of VBM and CBM at the grain boundaries? What could be the impact on optoelectronic properties?
- Explain how electrical doping can reduce the resistivity of a semiconductor.
- How do you think an annealing step could influence the type and doping level of $MAPbI_3$? Why?
- You process two $MAPbI_3$ films, one with 5% excess MAI and the second one with 5% excess PbI_2. What will be the impact on the optoelectronic properties of the film?

Sources used in this Lecture

- Ball, J.M., Petrozza, A. (2016). Defects in perovskite-halides and their effects in solar cells. *Nature Energy*, 1, 16149.
- Yin, W.-J., Shi, T., and Yan, Y. (2014). Unusual defect physics in $CH_3NH_3PbI_3$ perovskite solar cell absorber. *App. Phys. Lett.*, 104(6), 063903.
- Euvrard, J., Yan, Y., and Mizti, D.B. (2021). Electrical doping in halide perovskites. *Nat. Rev. Mat.*, 6(6), 531-549.
- Shi, T., Yin, W.-J., and Yan, Y. (2014). Predictions for p-Type CH3NH3PbI3 Perovskites. *The Journal of Physical Chemistry C*, 118(44), 25350-25354.